A comparative study on the morphology, structural, optical and electrical properties of ZnO nanostructures doped with different ions of group I, II, III, and transition element

WEILIANG FENG[a,b], CHENG WU[b], XIAOLING DUAN[c,*]
[a]*Key Laboratory of Green Chemical Process of Ministry of Education, Wuhan Institute of Technology, Wuhan 430073, China*
[b]*Key Laboratory of Novel Reactor and Green Chemical Technology of Hubei Province, Wuhan Institute of Technology, Wuhan 430073, China*
[c]*School of Chemical Engineering and Pharmacy, Wuhan Institute of Technology, Wuhan 430073, China*

The doped ZnO samples (group I, group II, group III, and transition mental element doped) were fabricated via solvothermal method with dimethylacetamide (DMAc) solvent. The comparison of the effects of different dopants on the morphological, microstructural, optical, and electrical properties of doped samples was investigated in detail. Compared to the pure sample, all doped ZnO samples showed high transparency in the visible range. The optical band gap obviously was decreased by doping. Furthermore, Urbach energy was calculated and discussed. The Urbach values indicated that the dopants may decrease the defect density of in the doped samples. The refractive index of the doped samples in the visible range showed different behavior. The resistivity of the obtained samples significantly depends on the doping types. The as-prepared Al-doped ZnO sample showed the lowest resistivity. At last, the photoluminescence exhibited the presence of a sharp ultraviolet emission and a broad blue emission at room temperature.

1. Introduction

ZnO is a polar inorganic crystalline material with many applications, mostly as electronic and photonic materials, because of its wide direct band gap of 3.37 eV [1, 2]. The wide band gap and large exciton binding energy make ZnO a promising candidate for low-voltage light emitting devices [3, 4]. In to develop efficient optoelectronic devices based on ZnO nanostructures at a lowest energy expense, effective methods to improve their visible light emission properties are highly desirable. Attempts have been made to modify or improve physico-chemical properties of the material, such as introducing dopants into ZnO to achieve multifunctionality [5]. The dopant types and concentration can have pronounced effects on the structural and electrical properties of ZnO microstructure [6]. In particular, a key requirement for many applications of optoelectronic devices is the doping of ZnO with various elements for enhancing and controlling its electrical and optical performance [7]. Till date, some reports have discussed the effects of different doping elements on the structural, optical, and electrical properties of ZnO samples obtained. Sharma et al. [8] studied the effects of Co-Mn dopants on ZnO nanoparticles prepared by co-precipitation method. They reported that ZnO samples doped with the mentioned elements obviously improved structural and optical properties. Musat et al. [9] investigated the properties of hydrothermal method derived ZnO nanostructures with Al dopant. They reported that the morphology and crystalline structure were strongly dependent on the Al-doping and growth temperature. Wu et al. [10] reported that Na-doped ZnO nanowires by a thermal decomposition route at temperature around 400ºC. The results showed that the low Na doping concentration contributed to the enhancement of the surface interstitial defects. As was expected and described above, the novel physico-chemical and photoelectric properties of new samples were brought by doping different elements. At present, the effects of the single element or congeners doping on the morphology, microstructural or optical properties of the new samples have been widely reported. However, the literature on comparative studies of group I, group II, group III, and transition mental element (TM) doping ZnO samples obtained by solovthermal method is still scanty. Especially, the comparison of the effects of different dopants on the morphological, microstructural, optical, and electrical properties of doped samples is only rarely reported. More in-depth studies are necessary to further understand their doping process, which can provide important information for its potential application in the optoelectronic devices.

Therefore, in this study, the doped ZnO samples

with commonly dopants (Na, Mg, Co, Mn, Ag, and Al) were fabricated by solvothermal method with N, N-Dimethylacetamide (DMAc) as a solvent and base. The ionic radius of the foreign elements were very close to those of Zn ionic. The comparison of the effects of different families of elements on the morphology, microstructural, optical properties, and electric properties of the new samples obtained has been studied and discussed in detail. This works also emphasized the importance of the optical, optoelectronic, and dielectric applications in controlling the optical and dielectric parameters of samples using dopants.

2. Experimental section

2.1. Synthesis of samples

Pure and doped ZnO samples were fabricated by a previous solvothermal method with DMAc as a solvent and base as reported in the literature [1]. The typical process was as follows: 0.02 M zinc acetate dihydrate and X (X=Na, Mg, Co, Mn, Ag, and Al) nitrate hydrate were dissolved in mixed solvent (DMAc:H_2O=1:4, v/v). The concentration of X doping was fixed at 3 wt.%. The growth process was carried out at 95 ℃ for 3 h. After the expected time the samples were cooled down to room temperature. The formed white precipitates were separated by centrifugation and washed thoroughly with deionized water. Subsequently, the white precipitates were dried in air at 80 ℃ overnight.

2.2. Characterization techniques

The morphologies and sizes of the samples were observed using scanning electron microscopy (S-4800, Hitachi). Phase composition of the as-synthesized samples was recorded by XRD (D8 Advance, Bruker) with CuKα (0.15406 nm) radiation source at 40 kV and 30 mA. FTIR spectrum was obtained using Bruker Tensor 27 spectrometer. In addition, the optical transmittance was measured using a UV-vis-NIR double beam spectrophotometer (Lamda 950, PE) in the wavelength range from 350 to 600 nm. The electrical resistance was measured by a four-point probe method (SDY-4, Guangzhou Semiconductor Research Institute). Finally, photoluminiscence (PL) measurements were carried out on a Varian Cary Eclipse spectrophotometer.

3. Results and discussion

3.1. Surface morphologies

The optical images of pure and doped ZnO samples are presented in Fig. 1. It can clearly observe that there are discrepancies among the colors of the samples obtained. The Ag doped sample exhibited yellow color. The light yellow color belongs to Al, Mn, and Mg doped samples. However, the color obtained for Na or Co dopant is very similar to that from the pure ZnO sample

(white color). The difference of the colors has further confirmed that the dopants may have played important roles in controlling their chemical and physical properties.
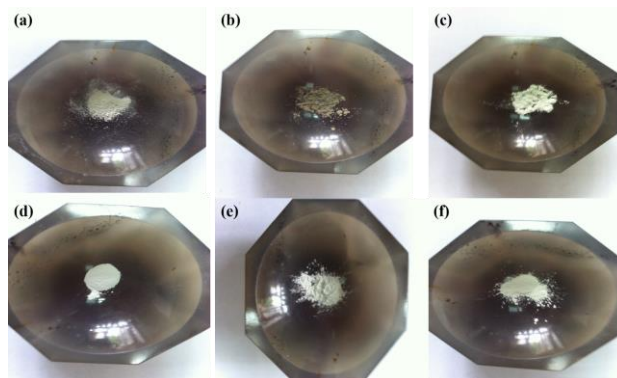
Fig. 1. The optical images of pure and doped ZnO.

Fig. 2 displays the morphologies of pure and doped ZnO samples with different doping elements. It was found that the morphologies of the synthesized ZnO samples are dependent largely on the dopant ion incorporated. It can be seen clearly that the samples with rod-like structures have been obtained for pure, Mn, and Ag-doped ZnO (Fig. 2a-c). The almost similar morphologies obtained for Mn and Ag-doped ZnO samples strongly suggested that the ZnO lattice was not much disturbed by the dopant ions. Structurally, wurtzite ZnO has two groups of polar planes, (0001) and (101'1) basal plane [11]. Under normal conditions, the growth velocity of (0001) plane is faster than other planes [12]. This fast anisotropic growth along c-axis direction of the wurtzite structure leads to the formation of ZnO rod-like shape crystals [13]. Doping of ZnO with Al and Na element remarkably changed the morphology of the structures from rod-like to tower-like (Fig. 2 d,e). The diameter of the rods gradually became smaller along the growth direction, leading to a tower-like structure with a sharp tip. The diameter varied from 800 nm at the bottom to about 200 nm at the tip. Understandably, the polar plane (0001) of ZnO usually preferably adsorb the complex growth units $Zn(OH)_4^{2-}$ in the solvent. The presence of the Al^{3+} ions instead of Zn^{2+} ions in the ZnO crystal is likely to enhance the adsorption of $Zn(OH)_4^{2-}$ ligands onto these basal surfaces, which cause an enhanced growth rate of ZnO nanocrystallites along the c-axis direction. It is well known that the more rapid the growth rate, the quicker the disappearance of the plane [14]. Hence, the (0001) plane gradually faded away during the doping process, and sharp tips were developed. In comparison with Fig. 2(a-e), it is clear that the ZnO samples with dumbbell-like structures were obtained using Mn or Co element as dopant (Fig. 2f, g). The dumbbell structured ZnO is consisted of two hexagonal ZnO microcrystal. The precise effects mechanism of the dopants (Na, Mg or Co) on the morphologies of samples obtained are now under investigation. On the basis of the investigations described above, it is reasonable to expect

that the different morphologies may be related to the effects of dopants, which might act as structure driving agents through selectively adsorbing onto ZnO crystalline planes [15].
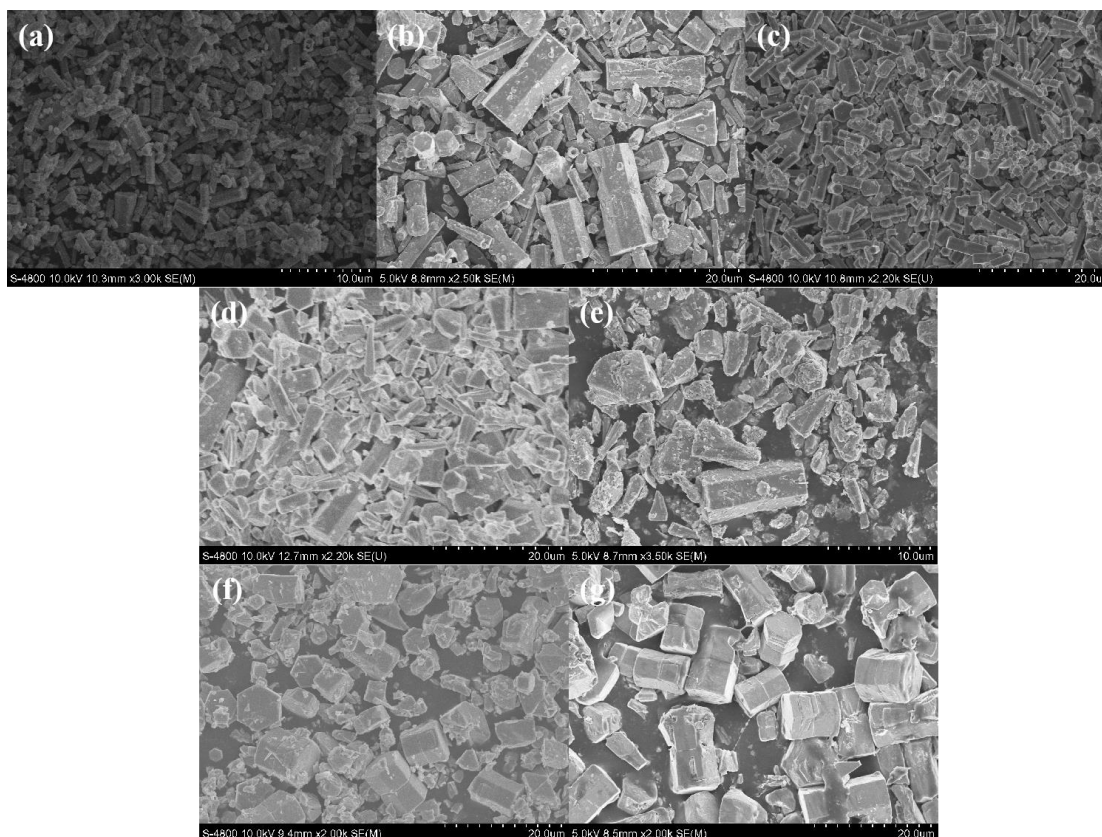
Fig. 2. The morphologies of pure and doped ZnO samples with different doping elements

3.2. Structural properties

Fig. 3 shows the typical XRD diffraction patterns collected from the doped and pure ZnO samples, in which the major peaks can be well assigned to those of hexagonal wurtzite ZnO (JCPDS No. 36-1451). There was no trace of any crystalline secondary phase (except for Ag-doping) which verified that most of the doping ions might have been substituted for Zn^{2+} or incorporated into the Zn^{2+} interstitial sites of the ZnO lattice. However, in the case of Ag-doped ZnO, a low intensity diffraction peak related to metallic Ag (JCPDS No. 04-0783) is identified. According to this novel phenomenon, it might be concluded that only a limited incorporation of Ag^+ ions into the ZnO lattice through substitution of Zn^{2+} ions could take place. This is likely due to the ionic radius

Ag^+ (1.15 Å) is larger than that of Zn^{2+} (0.74 Å) [16]. Even though the incorporation of Ag affects the crystal growth kinetics and surface energy of the doped ZnO crystals, it does not have any strong influence on the crystalline quality of ZnO nanostructures. In addition, although all the doped samples had similar diffraction patterns, it is possible to observe in Fig. 3a that the intensity of peaks varied with the presence of different dopants, indicating differences in crystallinity. At the same time, the (002) peak position of doped ZnO crystals slightly shifted to lower angles with the incorporation of dopants. This may be due to the fact that radius difference between the doping ionic and zinc ionic, which cause an expansion of the ZnO lattice parameter (Fig. 3b) [17].
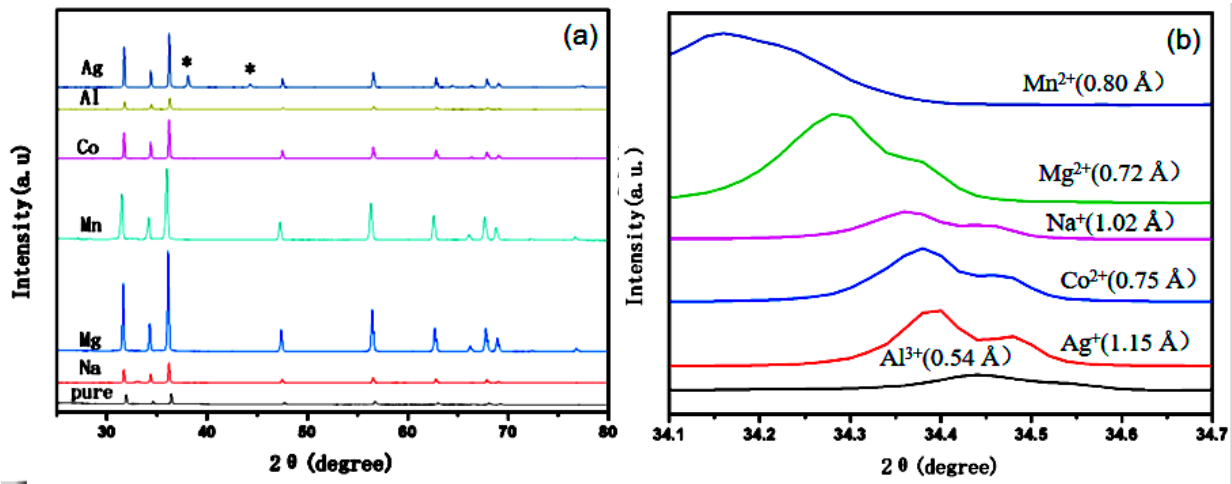
Fig. 3. The XRD diffraction patterns of pure and doped ZnO samples with different doping elements (color online)

3.3. FTIR Analysis

Fig. 4 shows the infrared spectrum of ZnO samples with different dopants. Similar spectrum was obtained for the pure ZnO as well as for the doped ZnO samples. For all doped ZnO samples the absorption peaks near 500 cm^{-1} could be attributed to Zn-O stretching vibration [18]. The peak near 3500 cm^{-1} is due to O-H stretching vibrations and the peak at 1600 cm^{-1} is due to the H-O-H bending vibration, all of which are associated with the small amount of H_2O molecules existing in the samples [19, 20]. However, the peak near 1400 cm^{-1} assigned to ν_{as} (CO) adsorbed from atmosphere.
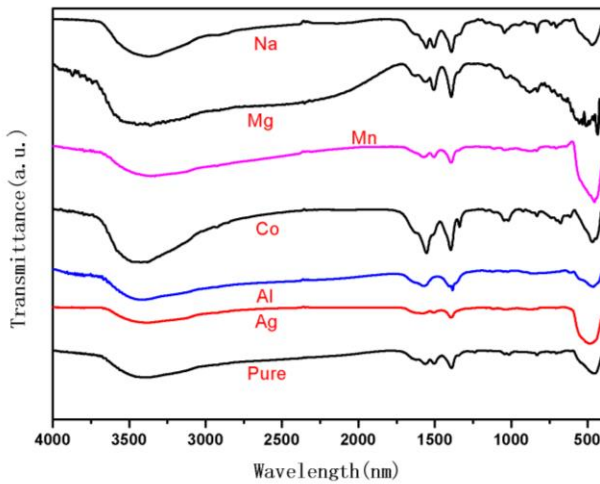
Fig. 4. The infrared spectrum of ZnO samples with different dopants (color online)

3.4. Optical properties

Fig. 5 shows the optical transmittance spectrum of pure and the doped samples in the entire range of 350-600 nm. The average optical transmittance in the visible range for pure ZnO sample was about 55.0%. However, the doped samples exhibited average transmittance values about 60%-75% and their

transmittance were higher than that of the pure ZnO sample.
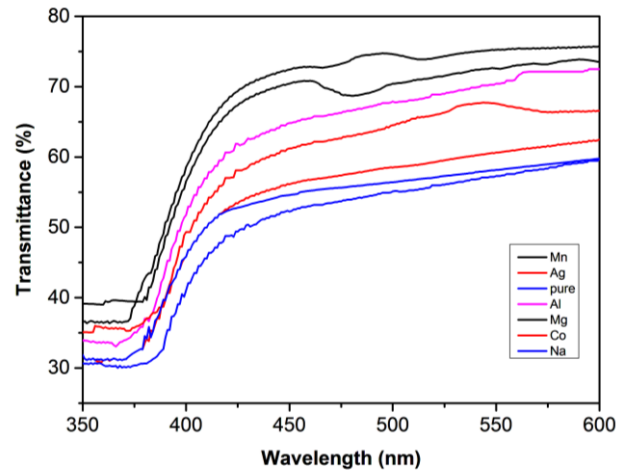
Fig. 5. The optical transmittance spectrum of pure and the doped samples in the entire range of 350-600 nm (color online)

The transmittance of the ZnO samples was effected by film thickness, surface roughness, grain size, and defects [21, 22]. In the present study, the increased transmittance of the doped ZnO rods is may be attributed to the reduction of surface roughness.

The absorption coefficient a can be calculated using the equation as [23, 24].

$$\alpha = -\ln T / d \tag{1}$$

where T is the transmittance, d is the film thickness. The optical band gap energy Eg of the doped samples can be determined by using the following equation [25]:

$$\alpha h\nu = A(h\nu - Eg)^{1/2} \tag{2}$$

where hv is the photon energy, A is a constant. The band

gap Eg values of the doped samples were evaluated and showed in the Fig. 6. It can be seen that the pure ZnO band gap is 3.22 eV. The value is close to that of previous reports [26, 27]. The Eg values of the doped ZnO samples are in the range of 3.05-3.21 eV, which are slightly less than that of the pure sample.
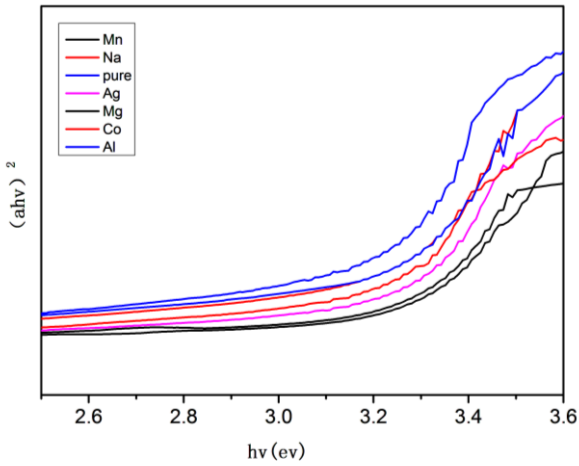
Fig. 6. The band gap Eg values of the doped samples with different doping elements (color online)

This band gap narrowing of transition metal doped II-IV semiconductor was likely to be interpreted in terms of sp-d spin exchange interactions between the conduction band electrons [28, 29]. However, for the non-transition metal doped ZnO in this study, a great majority of Na defects may induce impurity levels near the valence band maximum (VBM) and conduction band minimum (CBM), resulting in the decrease of band gap from 3.22 to 3.17 eV [30]. Bahsi [31] revealed that the band tails resulted from doping could lead to a large number of band-to-tail and tail-to-tail transitions and thus the absorption edge shifts to longer wavelength. As result of the incorporation of impurities into the semiconductor, the localized states available in the optical band gap of the doped samples effects the band gap structure and optical transitions which reveals a tail for the density of states of either one of the two band edge and the interactions with phonons [32]. The absorption edge may be follow the empirical Urbach rule [33, 34]:

$$\alpha = \alpha_0 e^{\frac{h\nu}{E_u}} \qquad (3)$$

where Eu represents an energy, a_0 is a constant. The Eu values were obtained from the reverse of the slope of ln(a) versus hv [35]. The Eu values from the samples obtained with different dopants are shown in the Fig. 7. It can be seen clearly that Eu values of the doped ZnO samples are in the range of 334.83-370.37 meV. This behavior may correspond to optical transitions between occupied states in the valence band tail to unoccupied states at the conduction band edge due to the density of defects and donor levels due to the interstitial Zn or doping atoms

[36]. It is reported that the increase in the Urbach energies values would lead to the formation of the doped samples with poor crystallinity [37]. With respect to pure sample, the doped samples showed lower Urbach energies. This means that the as-prepared doped samples have the good crystallinity, which was consistent with XRD diffraction patterns.
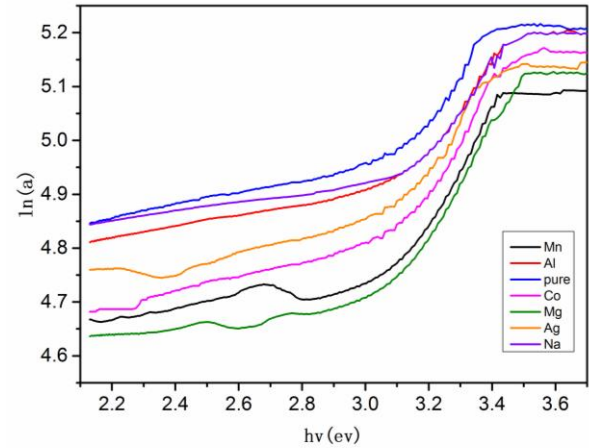
Fig. 7. The Eu values of the doped samples with different doping elements (color online)

The evaluation of refractive indices of optical materials is considerably important for the applications in integrated optic devices [38]. The refractive index n of the doped samples can be calculated using the following equation [39]:

$$n = \left[\frac{1+R}{1-R}\right] + \sqrt{\frac{4R}{(1-R)^2} - k^2} \qquad (4)$$

$$k = \frac{a\lambda}{4\pi} \qquad (5)$$

where R is the reflectance (Fig. 8), k is the extinction coefficient, λ is the wavelength of the incident photon and α is the absorption coefficient.
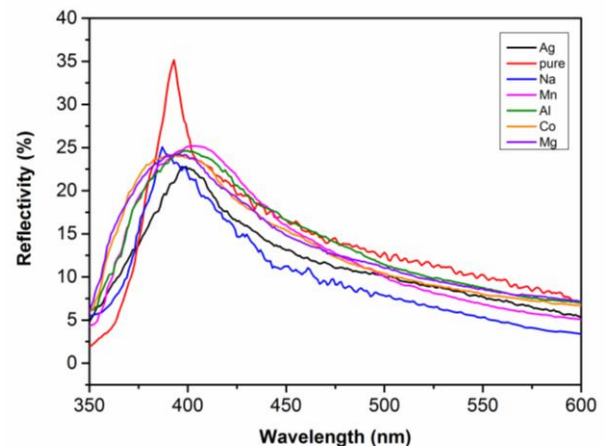
Fig. 8. The reflectance values of the doped samples with different doping elements (color online)

Fig. 9 shows the variation of the n values for different doped samples. As observed in Fig. 9, the n values decrease much more fast at about λ=350-500 nm. However, it shows different behavior for different doped samples. The refractive index of pure ZnO sample is about 1.9, which is close to that of the report [40]. However, it was found that the average refractive index of all the obtained samples in the visible range was about 1.52-2.26 for the system under study. Increasing or decreasing n is probably related to the compositional modifications due to the different dopants and level, which lead to increase or decrease in the optical quality of the films [41].
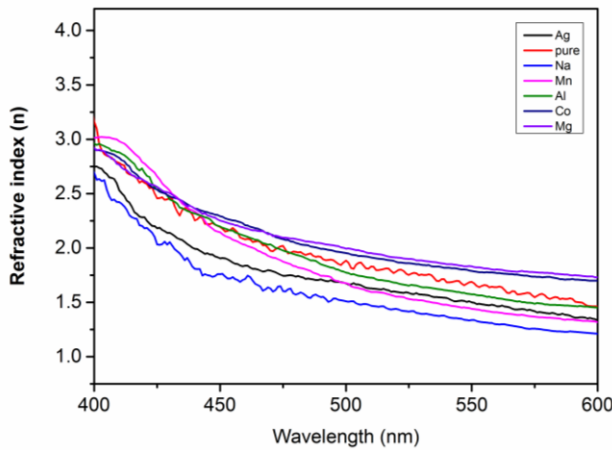
Fig. 9. The refractive values of the doped samples with different doping elements (color online)

The fundamental electron excitation spectrum of the doped samples was described by means of a frequency dependent of the complex electronic dielectric constant [42]. There was correlation between the values of the n and k and the dielectric constant of the materials [43]:

$$\varepsilon_r = n^2 - k^2 \qquad (6)$$

$$\varepsilon_i = 2nk \qquad (7)$$

where ε_r and ε_i are real and imaginary parts of the dielectric constant, respectively. These dielectric constant values for the doped ZnO samples were given in Fig. 10 (a, b). As seen in Fig. 10, the real part ε_r of all the samples are higher than that of imaginary part ε_i. The doped samples have a higher dielectric constant value (ε_r and ε_i) than the pure sample. For the TM doped samples, this can be attributed to the change in oxidation state of samples by interacting with Zn vacancy site that effect the charge imbalance, which leads to increase in polarizability of the system, especially in the nanocrystalline structures [44].
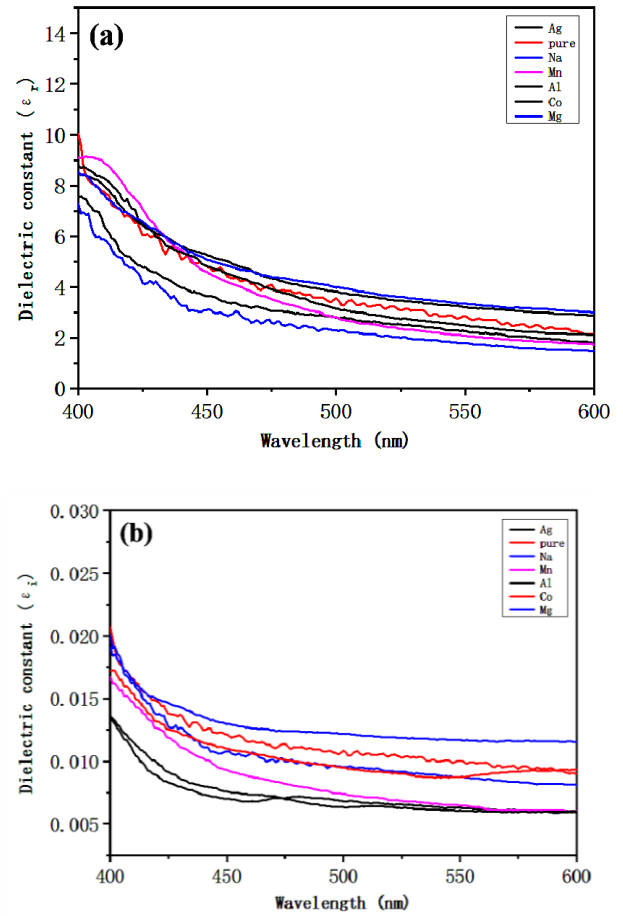
Fig. 10. The dielectric constant of the doped samples with different doping elements (color online)

Table 1 shows the typical electrical properties of pure and doped ZnO samples. It appeared that the electrical properties of doped ZnO samples were improved with the dopants in the study, which can be attributed to the reduction in the scattering of the carriers at the grain boundaries and crystal defects [45]. Among all the doped ZnO samples, the Al-doped sample exhibited the lowest resistivity, 9×10^3 Ωcm. The variation can be explained by the fact that the Al^{3+} ions substitutes for Zn^{2+} ions in ZnO crystal and supplies an abundance number of free electrons in the ZnO lattice, which cause the electrical conductivity increasing.

Table 1. The typical electrical properties of pure and doped ZnO samples

Samples	Resistivity (Ωcm)
Na-doped	5.2×10^4
Ag-doped	5.4×10^4
Pure ZnO	5.8×10^4
Mn-doped	3.6×10^4
Mg-doped	1.7×10^4
Co-doped	1.2×10^4
Al-doped	9×10^3

3.5. Photoluminescence spectroscopy

Optical absorption spectrum of pure and doped ZnO samples was recorded (Fig. 11). It can be seen that the PL spectrum of as-prepared ZnO samples has similar line-shape, and is consisted of two main parts: an intensive ultraviolet emission at 380 nm and a weak blue emission at 450 nm. Although all the samples exhibit similar position of the defect emission, differences in the UV to visible emission ratio can be observed. The absorption spectrum of Na-doped samples (Fig. 7) exhibited a strong absorption peak in the vicinity of the absorption edge from 362 nm to 380 nm. In addition, it can also be observed that the UV emission peak position is at slightly different position for different samples, which could be due to different native defect and free carrier concentrations in different samples [46]. However, a full understanding of the actual recombination mechanism of the defect-level emission band needs more experiments since their assignments are still under debate due to the complicated microscopic defects in ZnO.
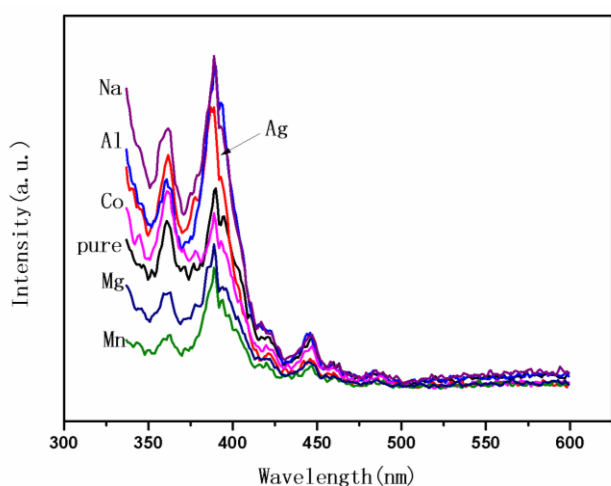
Fig. 11. Optical absorption spectrum of pure and doped ZnO samples (color online)

3.6. Applications

There are a few studies focused on solution phase synthesis of the doped ZnO materials. Wang et al. [30] synthesized Na doped ZnO thin films by sol-gel method. As Na doping content increases to 24 at.%, the average transmittance was still larger than 62% in the visible range. This is similar to the results in this report, but the concentration of element doping (24 at.%) is much larger than that of ours (3 at.%). Transparent and conductive high-preferential c-axis-oriented Al-doped zinc oxide thin films have been prepared [47]. The minimum sheet resistance of $10^4 \, \Omega/cm$ was obtained for the film doped with 1.6 mol% Al. With respect to the reported results, the Al-doped ZnO samples prepared in this paper showed lower resistivity values. Nevertheless, further work is ongoing to optimize the functional materials to facilitate their use in optoelectronic applications.

4. Conclusions

In conclusion, pure and doped ZnO (group I, group II, group III, and transition mental element doped) samples were successfully prepared by solvothermal method with DMAc solvent. SEM images showed that the incorporation of ions in crystal structure of ZnO can drastically change the morphology of ZnO samples from rods-like to dumbbell-like. XRD analysis showed that sharp and intense peaks, which indicating the doped samples were well crystallized. Compared to the pure sample, all doped ZnO samples showed high transparency in the visible range (>60%). The optical band gap values of doped ZnO samples were in the range of 3.05-3.21 eV. The Urbach values indicated that the dopants may be decrease the defect density of in the doped samples. The refractive index of the doped samples in the visible range showed different behavior. The resistivity of the obtained samples significantly depends on the doping types. The as-prepared Al-doped ZnO sample showed the lowest resistivity (9×10^3 Ωcm). At last, room temperature photoluminescence exhibited the presence of a sharp ultraviolet emissions and a broad blue emissions for the doped samples.

References

[1] W. L. Feng, P. Huang, B. C. Wang, C. W. Wang, W. G. Wang, T. L. Wang, S.F. Chen, R. L. Lv, Y. H. Qin, J. Y. Ma, Ceram. Int. **42**, 2250 (2016).
[2] W. L. Feng, B. C. Wang, P. Huang, X. D. Wang, J. Yu, C. W. Wang, Mat. Sci. Semicon. Proc. **41**, 462 (2016).
[3] V. M. Diep, A. M. Armani, Nano Lett. **16**, 7389 (2016).
[4] W. L. Feng, P. Huang, L. F. Jiang, Ceram. Int. **40**, 6383 (2014).
[5] F. L. Xian, L. H. Xu, X. X. Wang, X. Y. Li, Cryst. Res. Technol. **47**, 423 (2012).
[6] X. Li, Z. Hu, J. Liu, D. Li, X. Zhang, J. Chen, J. Fang, Appl. Catal. B **195**, 29 (2016).
[7] H. F. Li, Y. H. Huang, Q. Zhang, Y. Qiao, Y. S. Gu, J. Liu, Y. Zhang, Nanoscale **3**, 654 (2011).
[8] D. Sharma, R. Jha, J. Alloy. Compd. **698**, 532 (2017).
[9] V. Musat, M. Mazilu, N. Tigau, P. Alexandru, A. Dinescu, M. Purica, Thin Solid Films **617**, 120 (2016).
[10] C. Wu, Q. Huang, J. Lumin. **130**, 2136 (2010).
[11] W. L. Feng, P. Huang, Ceram. Int. **40**, 8963 (2014).

[12] H. Xu, L. Dong, X. Shi, Y. Liu, M. A. V. Hove, N. Lin, S. Y. Tong, J. Phys. Chem. C **120**, 26915 (2016).

[13] X. Bai, L. Yi, D. Liu, E. Nie, C. Sun, H. Feng, J. Xu, Y. Jin, Z. Jiao, X. Sun, Appl. Surf. Sci. **257**, 10317 (2011).

[14] A. Pimentel, J. Rodrigues, P. Duarte, D. Nunes, F. M. Costa, T. Monteiro, R. Martins, E. Fortunato, J. Mater. Sci. **50**, 5777 (2015).

[15] R. Zamiri, A. F. Lemos, A. Reblo, H. A. Ahangar, J. M. F. Ferreira, Ceram. Int. **40**, 523 (2014).

[16] S. Khosravi-Gandomani, R. Yousefi, F. Jamali-Sheini, N. M. Huang, Ceram. Int. **40**, 7957 (2014).

[17] A. Hui, J. Liu, J. Ma, Colloid. Surface. A **506**, 519 (2016).

[18] N. A. Aal, F. Alhazmi, A. A. Alghamdi, F. Eltantawy, F. Yakuphanoglu, Spectrochim. Acta A **135**, 871 (2015).

[19] S. Suwanboon, P. Amornpitoksuk, P. Bangrak, C. Randorn, Ceram. Int. **40**, 975 (2014).

[20] K. Zhou, Q. Zhang, Y. Shi, S. Jiang, Y. Hu, Z. Gui, J. Alloy Compd. **577**, 389 (2013).

[21] C. Y. Tsay, K. S. Fan, C. M. Lei, J. Alloy Compd. **512**, 216 (2012).

[22] Q. Feng, D. Tang, E. Jiang, S. Gu, S. Han, J. Alloy Compd. **578**, 228 (2013).

[23] S. Ilican, M. Caglar, Y. Caglar, Appl. Surf. Sci. **256**, 7204 (2010).

[24] W. T. Yen, Y. C. Lin, P. C. Yao, J. H. Ke, Y. L. Chen, Thin Solid Films **518**, 3882 (2010).

[25] P. Chand, A. Gaur, A. Kumar, J. Alloy Compd. **539**, 174 (2012).

[26] Z. N. Ng, K. Y. Chan, T. Tohsophon, Appl. Surf. Sci. **258**, 9604 (2012).

[27] N. Y. Mostafa, Z. K. Heiba, M. M. Ibrahim, J. Mol. Struct. **1079**, 480 (2015).

[28] Dhruvashi, P. K. Shishodia, Thin Solid Films **612**, 55 (2016).

[29] V. K. Jayaraman, A. M. Álvarez, Y. M. Kuwabara, Y. Koudriavstev, M. D. L. L. O. Amador, Mat. Sci. Semicon. Proc. **47**, 32 (2016).

[30] L. W. Wang, F. Wu, D. X. Tian, W. J. Li, L. Fang, C. Y. Kong, M. Zhou, J. Alloy. Compd. **623**, 367 (2015).

[31] Z. B. Bahsi, A. Y. Oral, Opt. Mater. **29**, 672 (2007).

[32] R. Mimouni, K. Boubaker, M. Amlouk, J. Alloy Compd. **624**, 189 (2015).

[33] S. J. Ikhmayies, R. N. Ahmad-Bitar, Journal of Matererials Research and Technology **2**, 221 (2013).

[34] K. Boubaker, Eur. Phys. J. Plus **126**, 1 (2011).

[35] S. Ilican, Y. Caglar, M. Caglar, M. Kundakci, A. Ates, Int. J. Hydrogen Energy **12**, 5201 (2009).

[36] R. Mimouni, O. Kamoun, A. Yumak, A. Mhamdi, K. Boubaker, P. Petkova, M. Amlouk, J. Alloy Compd. **645**, 100 (2015).

[37] A. M. E. Sayed, S. Taha, G. Said, A. A. Al-Ghamdi, F. Yakuphanoglu, Superlattice. Micros. **60**, 108 (2013).

[38] J. G. Lv, K. Huang, X. M. Chen, J. B. Zhu, C. B. Cao, X. P. Song, Z. Q. Sun, Opt. Commun. **284**, 2905 (2011).

[39] N. A. Subrahamanyam, A Textbook of Optics, Brj Laboratory, Delhi, 1977.

[40] R. G. Heideman, P. V. Lambeck, J. G. E. Gardeniers, Opt. Mater. **4**, 741 (1995).

[41] A. Goktas, F. Aslan, A. Tumbul, S. H. Gunduz, Ceram. Int. **43**, 704 (2017).

[42] Q. Xu, R. D. Hong, H. L. Huang, Z. F. Zhang, M. K. Zhang, X. P. Chen, Z. Y. Wu, Opt. Laser Technol. **45**, 513 (2013).

[43] H. Y. He, J. F. Huang, J. Fei, J. Lu, J. Mater. Sci: Mater. Electron. **26**, 1205 (2015).

[44] S. Singh, P. Dey, J. N. Roy, S. K. Mandal, J. Alloy. Comp. **642**, 15 (2015).

[45] V. Musat, B. Teixeira, E. Fortunato, R. C. C. Monteiro, Thin Solid Films **502**, 219 (2006).

[46] M. Y. Xie, N. Ben. Sedrine, S. Schoche, T. Hofmann, M. Schubert, L. Hung, B. Monemar, X. Wang, A. Yoshikawa, K. Wang, T. Araki, Y. Nanishi, V. Darakchieva, J. Appl. Phys. **115**, 163504 (2014).

[47] S. Y. Kuo, W. C. Chen, F. I. Lai, C. P. Cheng, H. C. Kuo, S. C. Wang, W. F. Hsieh, J. Cryst. Growth **287**, 78 (2006).

_____

*Corresponding author: duanxiaoling@hust.edu.cn